SAE 8620
Simulated Carburized Core
Iterations #120 and #144

Microstructural Data, Monotonic
And
Fatigue Test Results

Prepared by:

J. Lindsey
and
A. Fatemi

Department of Mechanical, Industrial and
Manufacturing Engineering
The University of Toledo
Toledo, Ohio 43606

Prepared for:
The AISI Bar Steel Applications Group

June 2010

American Iron and Steel Institute

American Iron and Steel Institute
2000 Town Center, Suite 320
Southfield, Michigan 48075
tel: 248-945-4777
fax: 248-352-1740
www.autosteel.org

TABLE OF CONTENTS

NOMENCLATURE

A_o, A_f	initial, final area	S	engineering stress
HB, HRB, HRC	Brinell, Rockwell B-Scale, Rockwell C-Scale Hardness number	YS, UYS, LYS, YS'	Monotonic yield, upper yield, lower yield, cyclic yield strength
b, c, n	fatigue strength, fatigue ductility, strain hardening exponent	YPE	yield point elongation
D_o, D_f	initial, final diameter	S_u	ultimate tensile strength
e	engineering strain	%EL	percent elongation
E, E'	monotonic, midlife cycle modulus of elasticity	%RA	percent reduction in area
K, K'	monotonic, cyclic strength coefficient	σ, σ_f, σ_f'	true stress, true fracture strength, fatigue strength coefficient
L_o, L_f	initial, final gage length	σ_a, σ_m, $\Delta\sigma$	stress amplitude, mean stress, stress range
$N_{50\%}$, $(N_f)_{10\%}$, $(N_f)_{50\%}$,	number of cycles to midlife, 10% load drop, 50% load drop,	ε_e, ε_p, ε	true elastic, plastic, total strain
$2N_f$	reversals to failure	ε_f, ε_f'	true fracture ductility, fatigue ductility coefficient
P_f, P_u	fracture, ultimate load	ε_a, ε_m, $\Delta\varepsilon$	strain amplitude, mean strain, strain range
R	strain ratio, neck radius	$\Delta\varepsilon_e$, $\Delta\varepsilon_p$	elastic, plastic strain range

NOMENCLATURE

$\sigma_{m, SC}$	small cycle mean stress	$\sigma_{a, SC}$	small cycle stress amplitude
$\sigma_{m, OL}$	overload cycle mean stress	$\sigma_{a, OL}$	overload cycle stress amplitude
$\varepsilon_{a, SC}$	small cycle strain amplitude	$(\Delta\varepsilon_p/2)_{SC}$	small cycle plastic strain amplitude,
$\varepsilon_{a, OL}$	overload cycle strain amplitude	$(\Delta\varepsilon_p/2)_{OL}$	overload plastic strain amplitude
$\varepsilon_{m, SC}$	small cycle mean strain	B, B_f	number of blocks in a periodic overload test, number of blocks to failure in a periodic overload test
N_{SC}, $N_{f, SC(eq)}$	number of small cycles in an overload block, calculated equivalent life of the small cycles in an overload test	$N_{f, OL}$	Constant amplitude life to failure at the strain amplitude used for the periodic overload cycle amplitude

UNIT CONVERSION TABLE

Measure	SI Unit	US Unit	from SI to US	from US to SI
Length	mm	in	1 mm = 0.03937 in	1 in = 25.4 mm
Area	mm^2	in^2	1 mm^2 = 0.00155 in^2	1 in^2 = 645.16 mm^2
Load	kN	klb	1kN = 0.2248 klb	1 klb = 4.448 kN
Stress	MPa	ksi	1 MPa = 0.14503 ksi	1 ksi = 6.895 MPa
Temperature	^oC	^oF	$^oC = (^oF - 32)/1.8$	$^oF = (^oC * 1.8) + 32$

In SI Unit:				
	1 kN = 10^3 N	1 Pa = 1 N/m^2	1 MPa = 10^6 Pa = 1 N/mm^2	1 Gpa = 10^9 Pa
In US Unit:				
	1 klb = 10^3 lb	1 psi = 1 lb/in^2	1 ksi = 10^3 psi	

SUMMARY

Monotonic tensile properties and fatigue behavior data were obtained for the steel material of iteration 120. The material was provided by AISI. Two tensile tests were performed to acquire the desired monotonic properties. Both tests gave similar results. Eighteen strain-controlled fatigue tests were performed to obtain the fatigue life and cyclic deformation curves and properties. The experimental procedure followed and results obtained are presented and discussed in this report. For iteration 144, periodic overload fatigue behavior and data were obtained from eight periodic overload fatigue tests. The experimental procedure followed and results obtained from periodic overload tests are also presented and discussed in this report.

I. EXPERIMENTAL PROGRAM

1.1 Material and Specimen Fabrication

1.1.1 Material

The steel material was provided by AISI. The test specimens were prepared from an 8620 steel grade. The samples were heat treated by austenitizing at 1700F for three and a half hours before lowering the temperature to 1600F for forty minutes. Quenching was performed in 140F oil and then tempering at 350F to an aim hardness of 36 HRC. This heat treatment procedure was used to simulate a carburizing cycle. Microstructure of the material is shown in Figures 1 and 2.

1.1.2 Specimen

In this study, identical round specimens were used for monotonic and fatigue tests. The specimen configuration and dimensions are shown in Figure 3. This configuration deviates slightly from the specimen geometry recommended by ASTM Standard E606 [1]. The recommended specimens have uniform gage sections. The specimen geometry shown in Figure 3 differs by using a large secondary radius in the gage section to compensate for the slight stress concentration at the gage to grip section transition.

Before heat treatment, specimen blanks were machined from bars of SAE 8620 as-hot rolled steel. Each specimen blank was cut to a length of 5.5 inches and the diameter was reduced from the starting bar diameter of 2.105 inches to 0.75 inches.

After heat treatment, final machining of the specimen was performed in the Mechanical, Industrial, and Manufacturing Engineering Machine Shop at the University of Toledo. The specimens were initially turned on a lathe to an appropriate diameter for insertion into a CNC/milling machine. Using the CNC machine, final turning was performed to achieve the tolerable dimensions specified on the specimen drawings.

The specimens were then polished prior to testing at the University of Toledo. A commercial round-specimen polishing machine was used to polish the specimen gage section. Three different grits of aluminum oxide lapping film 30 μm, 12 μm, and 3 μm were used. Polishing marks coincided with the longitudinal direction of the specimen. The polished surfaces were carefully examined under magnification to ensure complete removal of machine marks within the test section.

1.2 Testing Equipment

1.2.1 Apparatus

An INSTRON 8801 closed-loop servo-controlled hydraulic axial load frame in conjunction with a Fast-Track digital servo-controller was used to conduct the tests. The load cell used had a capacity of 50 kN. Hydraulically operated grips using universal tapered collets were employed to secure the specimens' ends in series with the load cell.

Total strain was controlled using an extensometer rated as ASTM class B2 [2]. The calibration of the extensometer was verified using displacement apparatus containing a micrometer barrel in divisions of 0.0001 in. The extensometer had a gage length of 0.30 in. and was capable of measuring strains up to 15 %.

In order to protect the specimens' surface from the knife-edges of the extensometer, ASTM Standard E606 recommends the use of transparent tape or epoxy to 'cushion' the attachment. For this study, it was found that application of transparent tape allowed for more consistency of the material thickness between the knife edge and the specimen. Therefore, transparent tape was considered to be the best protection. The tests were performed using three layers of transparent tape.

1.2.2 Alignment

Significant effort was put forth to align the load train (load cell, grips, specimen, and actuator). Misalignment can result from both tilt and offset between the central lines of the load train components. In order to align the machine, a round strain-gage bar was used. The Strain-gage bar has two arrays of four strain gages per array with one array arranged at the upper and lower ends of the uniform gage section. This was done in accordance with ASTM Standard E1012 [3].

1.3 Test Methods and Procedures

1.3.1 Monotonic tension tests

Monotonic tests in this study were performed using test methods specified by ASTM Standard E8 [4]. Two specimens were used to obtain the monotonic properties.

In order to protect the extensometer, strain control was used only up to 10% strain, until the point of ultimate tensile strength had been crossed. After this point, displacement control was used until fracture. INSTRON Bluehill software was used for the monotonic tests. For the elastic and initial yield region (0% to 1% strain) a strain rate of 0.0025 mm/mm/min was chosen. This strain rate was about one half of the maximum allowable rate specified by ASTM Standard E8 for the initial yield region. After the strain reached 1% a strain rate of 0.005 mm/mm/min was used up until the extensometer was removed. This strain rate was ten percent of the maximum allowable rate specified by ASTM Standard E8 for the region after yielding. After the extensometer was removed, a displacement rate of 0.2 mm/min was used.

After the tension tests were concluded, the broken specimens were carefully reassembled. The final gage lengths of the fractured specimens were measured with a Vernier caliper having divisions of 0.001 in. Using an optical comparator with 10X magnification and divisions of 0.001 in, the final diameter and neck radius were measured. It should be noted that prior to the test, the initial diameter was measured with this same instrument.

1.3.2 Constant amplitude fatigue tests

All constant amplitude fatigue tests in this study were performed according to ASTM Standard E606. It is recommended by this standard that at least 10 specimens be used to generate the fatigue properties. For this study, 18 specimens at 6 different strain amplitudes ranging from 0.225% to 2.000% were utilized. INSTRON SAX software was used in all strain-controlled tests. During each strain-controlled test, the total strain was recorded using the extensometer output. Test data were automatically recorded throughout each test.

There were two control modes used for these tests. Strain control was used in all tests with plastic deformation. For one of the elastic tests, strain control was used initially to determine the stabilized load, then load control was used for the remainder of the test and for the rest of the elastic tests, load control was used throughout. The reason for the change in control mode was due to the frequency limitation on the extensometer. For the strain-controlled tests, the applied frequencies ranged from 0.2 Hz to 3 Hz in order to keep a strain rate about 0.02 in/in/sec. For the load-controlled tests, load waveforms with frequencies of up to 35 Hz were used in order to shorten the overall test duration. All tests were conducted using a triangular waveform except the tests run at 35 Hz, when a sinusoidal waveform was used.

1.3.3 Periodic overload fatigue tests

The overload tests were conducted to investigate the effects of periodic overloads on the fatigue life of smaller subsequent cycles. For this study, 8 specimens were tested at 4 different strain amplitudes. All eight of the tests were performed in load-control after the initial pre-cycles in strain-control. The periodic overload tests were performed with INSTRON WAVERUNNER software. During each test, the total strain was recorded using the extensometer output. Test data were automatically recorded throughout each test.

The input signal consisted of a periodic fully reversed overload of the type shown in Figure 13. The load history in these tests consisted of repeated blocks made up of one fully-reversed overload cycle followed by a group of smaller constant amplitude cycles having the same maximum stress as the overload cycle. The overload cycles were applied at frequent intervals to maintain a larger effective strain range resulting in the subsequent cycles being fully effective.

With this overload history, as the large cycles become more frequent, the fraction of the total damage done by them increases and that done by the small cycles decreases. The fully reversed strain amplitude for the overload cycle corresponded to about 10^4

cycles to failure. The number of small cycles per block, N_{sc}, were adjusted so that they cause 80% to 90% of the damage per block. Small cycle strain levels were selected at or below the run out level of the constant amplitude tests. Small cycle strain amplitudes were used from 0.085% to 0.175% and the number of small cycles per overload cycle ranged between 64 and 2048.

For the load-controlled tests, calculations were performed based on equation 6 in order to arrive at the steady state stress amplitudes for the desired strain amplitudes. Due to the transient response of the material, the calculated loads would result in a lower than expected strain amplitude throughout the test. In order to reduce cyclic transient behavior, 1000 strain-controlled pre-cycles were applied at the periodic overload strain level.

After completion of these initial cycles the second portion of the test was started using the previously mentioned periodic overload history. Eight load-controlled tests were performed at four load levels with expected strain levels from 0.175% to 0.085%.

II. EXPERIMENTAL RESULTS AND ANALYSIS

2.1 Microstructural Data

A specimen was sectioned longitudinally from the grip end to obtain a general microstructure description. The sample was prepared with standard test procedures for sectioning, mounting, polishing, and etched with 3% nital. The sample was reviewed and microphotographs were taken using an Olympus PMG3 Microscope. The microphotographs revealed that the entire sample consisted of martensite and transformation products. The chemistry of the material is presented in Table 1. Figures 1 and 2 show magnified views of the microstructure from a longitudinal section of the grip end of a tensile specimen. The complete material report for this steel was provided by the Chrysler Materials Engineering Lab and is attached as Appendix B of this report.

2.2 Monotonic Deformation Behavior

The properties determined from monotonic tests were the following: modulus of elasticity (E), yield strength (YS), ultimate tensile strength (S_u), percent elongation (%EL), percent reduction in area (%RA), true fracture strength (σ_f), true fracture ductility (ε_f), strength coefficient (K), and strain hardening exponent (n).

True stress (σ), true strain (ε), and true plastic strain (ε_p) were calculated from engineering stress (S) and engineering strain (e), according to the following relationships which are based on constant volume assumption:

$$\sigma = S(1+e) \qquad \text{(1a)}$$

$$\varepsilon = \ln(1+e) \qquad \text{(1b)}$$

$$\varepsilon_p = \varepsilon - \varepsilon_e = \varepsilon - \frac{\sigma}{E} \tag{1c}$$

The true stress (σ) - true strain (ε) plot is often represented by the Ramberg-Osgood equation:

$$\varepsilon = \varepsilon_e + \varepsilon_p = \frac{\sigma}{E} + \left(\frac{\sigma}{K}\right)^{\frac{1}{n}} \tag{2}$$

The strength coefficient, K, and strain hardening exponent, n, are the intercept and slope of the best line fit to true stress (σ) versus true plastic strain (ε_p) data in log-log scale:

$$\sigma = K\left(\varepsilon_p\right)^n \tag{3}$$

In accordance with ASTM Standard E739 [5], when performing the least squares fit, the true plastic strain (ε_p) was the independent variable and the true stress (σ) was the dependent variable. These plots for the two tests conducted are shown in Figure 4. To generate the K and n values, the range of data used in this figure was chosen according to the definition of discontinuous yielding specified in ASTM Standard E646 [6]. Therefore, the valid data range occurred between the end of yield point extension and the strain at maximum load.

The true fracture strength was corrected for necking according to the Bridgman correction factor [7]:

$$\sigma_f = \frac{\dfrac{P_f}{A_f}}{\left[1+\dfrac{4R}{D_f}\right]\ln\left[1+\dfrac{D_f}{4R}\right]} \tag{4}$$

where P_f is load at fracture, R is the neck radius, and D_f is the diameter at fracture.

The true fracture ductility, ε_f, was calculated from the relationship based on constant volume:

$$\varepsilon_f = \ln\left(\frac{A_o}{A_f}\right) = \ln\left(\frac{1}{1 - RA}\right) \tag{5}$$

where A_f is the cross-sectional area at fracture, A_o is the original cross-sectional area, and RA is the reduction in area.

A summary of the monotonic properties for this material is provided in Table 2. The monotonic stress-strain curves are shown in Figure 5. As can be seen from this figure, the two curves are close to each other. Refer to Table A-1 for a summary of the monotonic test results.

2.3 Cyclic Deformation Behavior

2.3.1 Transient cyclic response

Transient cyclic response describes the process of cyclic-induced change in deformation resistance of a material. Data obtained from constant amplitude strain-controlled fatigue tests were used to determine this response. Plots of stress amplitude variation versus applied number of cycles can indicate the degree of transient cyclic softening/hardening. Also, these plots show when cyclic stabilization occurs. A composite plot of the transient cyclic response for the steel studied is shown in Figure A-1. The transient response is normalized on the rectangular plot in Figure A-1a, while a semi-log plot is shown in Figure A-1b. Even though multiple tests were conducted at each strain amplitude, data from one test at each strain amplitude tested is shown in these plots.

2.3.2 Steady-state cyclic deformation

Another cyclic behavior of interest was the steady state or stable response. Data obtained from constant amplitude strain-controlled fatigue tests were also used to determine this response. The properties determined from the steady-state hysteresis loops were the following: cyclic modulus of elasticity (E'), cyclic strength coefficient (K'), cyclic strain hardening exponent (n'), and cyclic yield strength (YS'). Half-life (midlife) hysteresis loops and data were used to obtain the stable cyclic properties.

Similar to monotonic behavior, the cyclic true stress-strain behavior can be characterized by the Ramberg-Osgood type equation:

$$\frac{\Delta \varepsilon}{2} = \frac{\Delta \varepsilon_e}{2} + \frac{\Delta \varepsilon_p}{2} = \frac{\Delta \sigma}{2E} + \left(\frac{\Delta \sigma}{2K'}\right)^{\frac{1}{n'}} \tag{6}$$

It should be noted that in Equation 6 and the other equations that follow, E is the average modulus of elasticity that was calculated from the monotonic tests.

The cyclic strength coefficient, K', and cyclic strain hardening exponent, n', are the intercept and slope of the best line fit to true stress amplitude ($\Delta\sigma/2$) versus true plastic strain amplitude ($\Delta\varepsilon_p/2$) data in log-log scale:

$$\frac{\Delta \sigma}{2} = K' \left(\frac{\Delta \varepsilon_p}{2}\right)^{n'} \tag{7}$$

In accordance with ASTM Standard E739 [5], when performing the least squares fit, the true plastic strain amplitude ($\Delta\varepsilon_p/2$) was the independent variable and the stress amplitude ($\Delta\sigma/2$) was the dependent variable. The true plastic strain amplitude was calculated by the following equation:

$$\frac{\Delta\varepsilon_p}{2} = \frac{\Delta\varepsilon}{2} - \frac{\Delta\sigma}{2E} \tag{8}$$

This plot is shown in Figure 6. To generate the K' and n' values, the range of data used in this figure was chosen for $\left[\frac{\Delta\varepsilon_p}{2}\right]_{calculated} \geq 0.0006$ in/in.

The cyclic stress-strain curve reflects the resistance of a material to cyclic deformation and can be vastly different from the monotonic stress-strain curve. The cyclic stress-strain curve is shown in Figure 7. In Figure 8, superimposed plots of monotonic and cyclic curves are shown. As can be seen in this figure, the material cyclically softened. Figure A-2 shows a composite plot of the steady-state (midlife) hysteresis loops. Even though multiple tests were conducted at each strain amplitude, the stable loops from only one test at each strain amplitude are shown in this plot.

2.4 Constant Amplitude Fatigue Behavior

Constant amplitude strain-controlled fatigue tests were performed to determine the strain-life curve. The following equation relates the true strain amplitude to the fatigue life:

$$\frac{\Delta\varepsilon}{2} = \frac{\Delta\varepsilon_e}{2} + \frac{\Delta\varepsilon_p}{2} = \frac{\sigma_f'}{E}\left(2N_f\right)^b + \varepsilon_f'\left(2N_f\right)^c \tag{9}$$

where σ_f' is the fatigue strength coefficient, b is the fatigue strength exponent, ε_f' is the fatigue ductility coefficient, c is the fatigue ductility exponent, E is the monotonic modulus of elasticity, and $2N_f$ is the number of reversals to failure.

The fatigue strength coefficient, σ_f', and fatigue strength exponent, b, are the intercept and slope of the best line fit to true stress amplitude ($\Delta\sigma/2$) versus reversals to failure ($2N_f$) data in log-log scale:

$$\frac{\Delta\sigma}{2} = \sigma_f'(2N_f)^b \tag{10}$$

In accordance with ASTM Standard E739, when performing the least squares fit, the stress amplitude ($\Delta\sigma/2$) was the independent variable and the reversals to failure ($2N_f$) was the dependent variable. This plot is shown in Figure 9. To generate the σ_f' and b values, all data, with the exception of the run-out tests, in the stress-life figure were used.

The fatigue ductility coefficient, ε_f', and fatigue ductility exponent, c, are the intercept and slope of the best line fit to calculated true plastic strain amplitude ($\Delta\varepsilon_p/2$) versus reversals to failure ($2N_f$) data in log-log scale:

$$\left(\frac{\Delta\varepsilon_p}{2}\right)_{calculated} = \varepsilon_f'(2N_f)^C \tag{11}$$

In accordance with ASTM Standard E739, when performing the least squares fit, the calculated true plastic strain amplitude ($\Delta\varepsilon_p/2$) was the independent variable and the reversals to failure ($2N_f$) was the dependent variable. The calculated true plastic strain amplitude was determined from Equation 8. This plot is shown in Figure 10. To generate the ε_f' and c values, the range of data used in this figure was chosen for $\left[\frac{\Delta\varepsilon_p}{2}\right]_{calculated} \geq 0.0006$ in/in.

The true strain amplitude versus reversals to failure plot is shown in Figure 11. This plot displays the strain-life curve (Eqn. 9), the elastic strain portion (Eqn. 10), the plastic strain portion (Eqn. 11), and superimposed fatigue data. A summary of the cyclic properties for this steel is provided in Table 2. Table A-2 provides the summary of the fatigue test results.

A parameter often used to characterize fatigue behavior at stress concentrations, such as at the root of a notch, is Neuber parameter [7]. Neuber's stress range is given by:

$$\sqrt{(\Delta\varepsilon)(\Delta\sigma)E} = 2\sqrt{(\sigma_f')^2(2N_f)^{2b} + \sigma_f'\varepsilon_f'E(2N_f)^{b+c}} \tag{12}$$

A plot of Neuber stress range versus reversals to failure is shown in Figure 12. This figure displays the Neuber curve based on Eqn. 12 and superimposed fatigue data for this material

2.5 Periodic Overload Fatigue Behavior

Periodic Overload fatigue tests were performed to determine the effective strain-life curve. The effective strain-life curve is plotted using the strain amplitude of the small cycles in the overload block and the calculated equivalent life. The equivalent fatigue life for the smaller cycles was obtained using the linear damage rule:

$$\frac{N_{OL}}{N_{f,OL}} + \frac{N_{SC}}{N_{f,SC(eq)}} = 1 \tag{13}$$

where N_{OL} is the number of overload cycles in a periodic overload test, $N_{f,OL}$ is the number of cycles to failure if only overloads were applied in a test, N_{SC} is the number of smaller cycles in a periodic overload test, and $N_{f,SC(eq)}$ is the computed equivalent fatigue life for the smaller cycles.

The linear damage rule was also used to calculate the cumulative damage of the overload cycles, D_{OL}, as

$$\frac{N_{OL}}{N_{f,OL}} = D_{OL} \tag{14}$$

Figure 14 shows the effective strain-life data superimposed on the constant amplitude strain life plot. Table A-3 presents a summary of the periodic overload test results.

A plot of the SWT parameter for both the constant amplitude and overload data provides another method of comparison between the two sets of data, where the mean stress present in the small cycles is taken into account. The SWT parameter is given by

$$\sigma_{\max}\varepsilon_a = \frac{1}{E}[(\sigma_f')^2(2N_f)^{2b} + \sigma_f'\varepsilon_f'E(2N_f)^{b+c}] \tag{15}$$

where $\sigma_{\max} = \sigma_m + \sigma_a$. The SWT plot is shown in Figure 15. As in the constant amplitude strain-life curve, the overload data and effective strain-life curve diverged from the constant amplitude curve.

Table 1: Chemical Composition of 8620 Steel (Courtesy of Gerdau-MacSteel)

Element	**Wt. %**
Carbon, C	0.22%
Manganese, Mn	0.83%
Silicon, Si	0.25%
Chromium, Cr	0.50%
Nickel, Ni	0.45%
Molybdenum, Mo	0.18%
Copper, Cu	0.20%
Phosphorus, P	0.006%
Sulfur, S	0.023%
Aluminum, Al	0.027%
Tin, Sn	0.007%
Vanadium, V	0.003%
Niobium, Nb	0.002%
Boron, B	0.0002%
Calcium, Ca	0.0007%
Titanium, Ti	0.0020%
Lead, Pb	0.0003%
Zirconium, Zr	0.0010%
DI	2.12%

Table 2: Summary of the Mechanical Properties

Microstructural Data	Average
ASTM grain size number (MAG=500X):	
First longitudinal direction (L-T)	Fine grain 5 - 8
Inclusion rating number (MAG=100x): (Provided by Macsteel Company)	
Type A (sulfide type), thin series	-
Type B (alumina type), thin & heavy series	-
Type C (silicate type, thin & heavy series	-
Type D (globular type), thin & heavy series	-
Hardness:	
Brinell (HB)(converted)	
the first longitudinal direction	352
Transverse direction	341
Rockwell B-scale (HRB)	
The first longitudinal direction	-
Transverse direction	-
Rockwell C-scale (HRC)(measured)	
The first longitudinal direction	38
Transverse direction	37
Microstructure type:	
The first longitudinal direction	Martensite & Transformation Products
Transverse direction	

Monotonic Properties	Average		Range					
Modulus of elasticity, E, GPa (ksi):	210.3	(30,497)	211.6	-	209.0	(30,684.6	-	30,310.4)
Yield strength (0.2% offset), YS , MPa (ksi):	795.8	(115)	796.0	-	795.5	(115.4	-	115.4)
Upper yield strength UYS, MPa (ksi):								
Lower yield strength LYS, MPa (ksi):								
Yield point elongation, YPE (%):								
Ultimate strength, S_u , MPa (ksi):	1145.2	(166)	1128.4	-	1162.1	(163.7	-	168.5)
Percent elongation, %EL (%):	35.5%		33.6%	-	37.3%			
Percent reduction in area, %RA (%):	50.8%		48.5%	-	53.2%			
Strength coefficient, K , MPa (ksi):	2,132.3	(309.3)	2,244.2	-	2,020.5	(325.5	-	293.0)
Strain hardening exponent, n:	0.1651		0.1741	-	0.1561			
True fracture strength, σ_f, MPa (ksi):	1585.7	(230.0)	1618.1	-	1553.4	(234.7	-	225.3)
True fracture ductility, ε_f (%):	71.1%		66.3%	-	75.9%			

Cyclic Properties	Average		Range					
Cyclic modulus of elasticity, E' , GPa (ksi):	210.1	(30,473)	214.5	-	202.3	(31,106.5	-	29,340.7)
Fatigue strength coefficient, σ_f' , MPa (ksi):	1,910.2	(277.0)						
Fatigue strength exponent, b:	-0.1028							
Fatigue ductility coefficient, ε_f' :	0.595							
Fatigue ductility exponent, c:	-0.5871							
Cyclic strength coefficient, K' , MPa (ksi):	2,078.1	(301.4)						
Cyclic strain hardening exponent, n':	0.1739							
Cyclic yield strength, YS', MPa (ksi)	705.3	(102.3)						
Fatigue Limit (defined at 10^6 cycles), Mpa (ksi)	430.2	(62.4)						

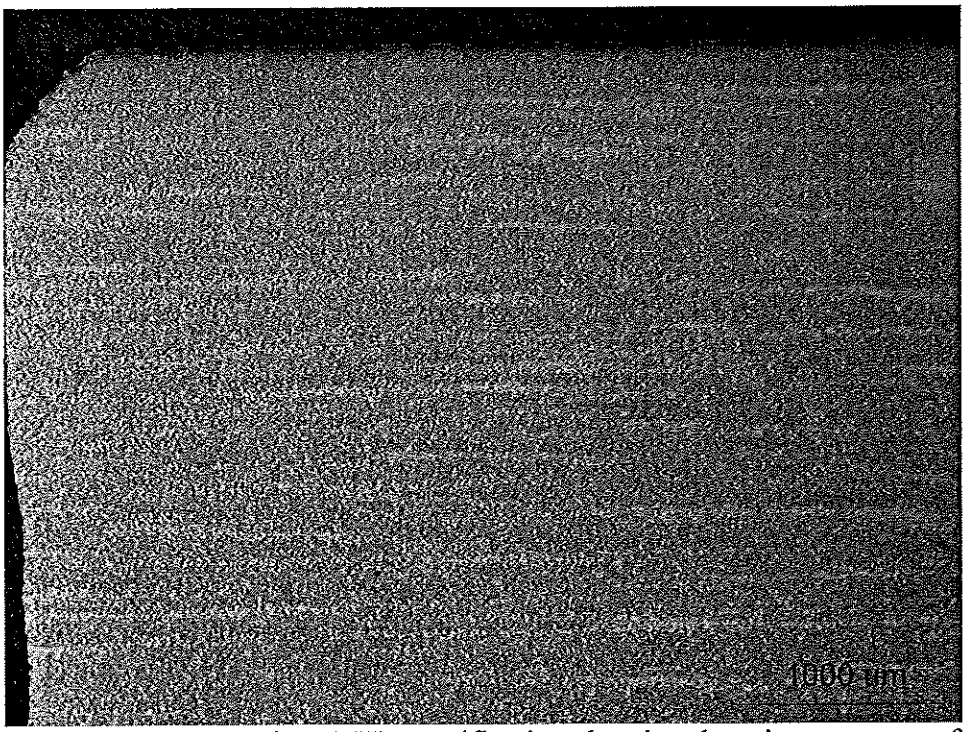

Figure 1: Micrograph at 15X magnification showing the microstructure of a longitudinal section from the grip area of a tensile specimen. (Courtesy of Chrysler)

Figure 2: Micrograph at 500X magnification showing the microstructure of a longitudinal section from the grip area of a tensile specimen. (Courtesy of Chrysler)

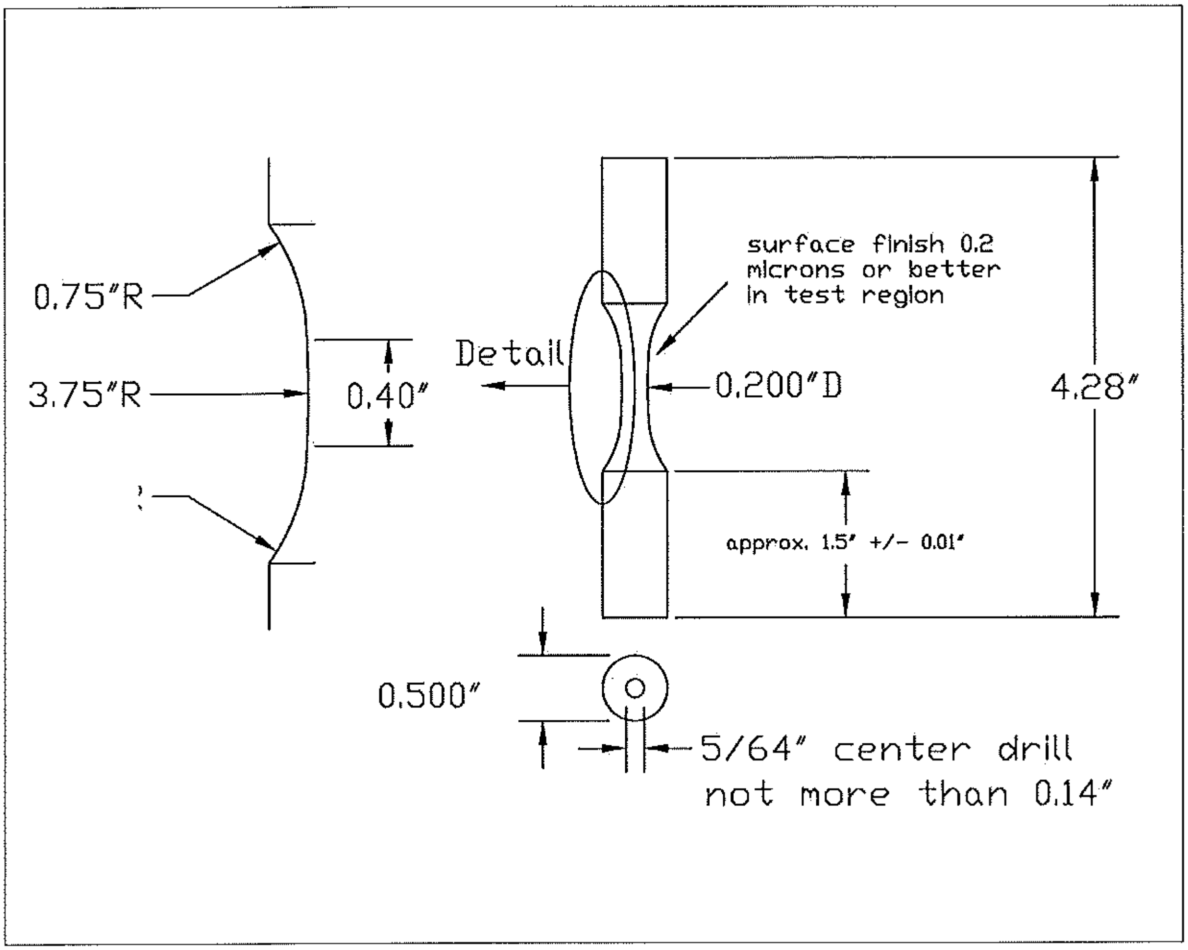

Figure 3: Specimen configuration and dimensions (in.)

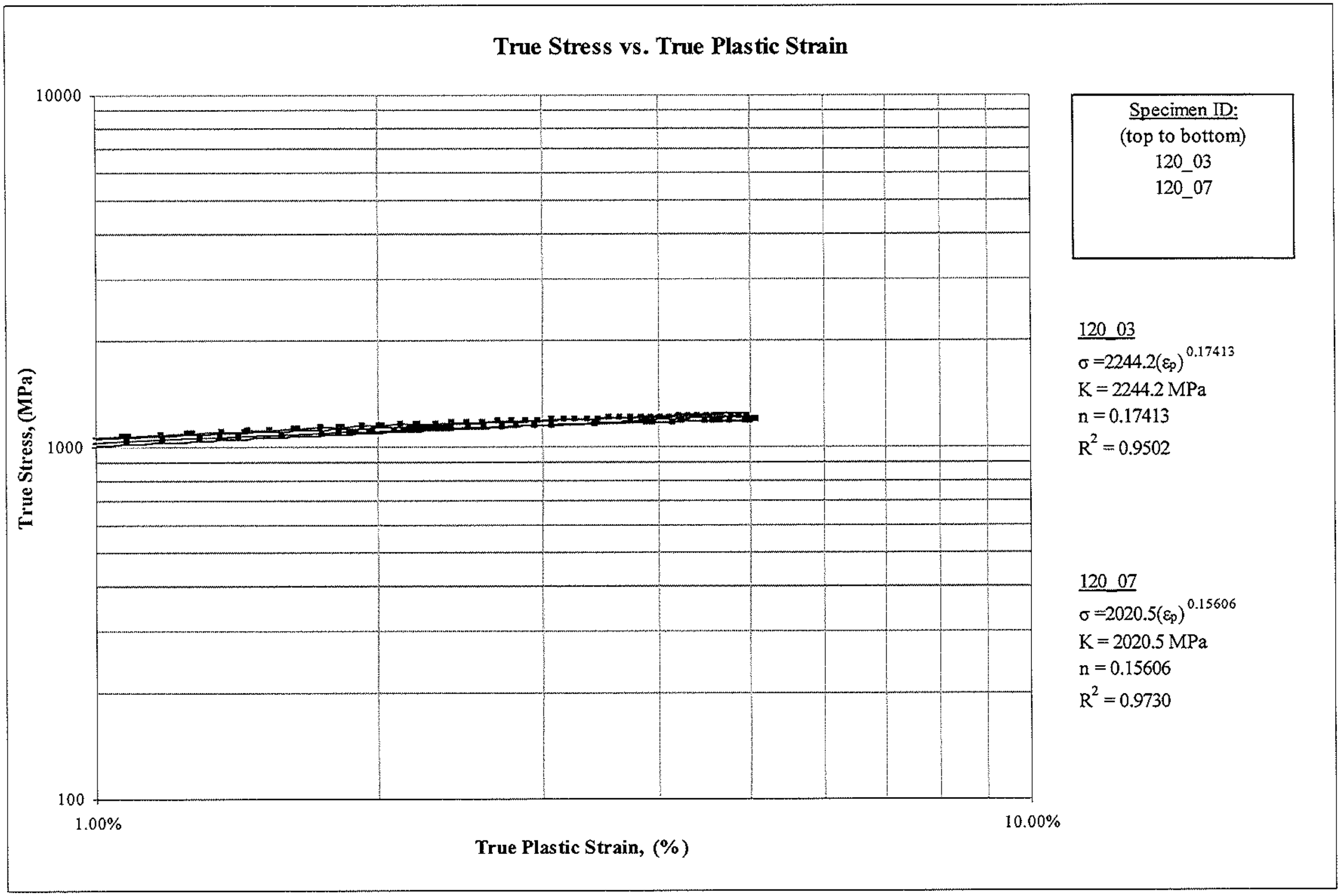

Figure 4: True stress versus true plastic strain

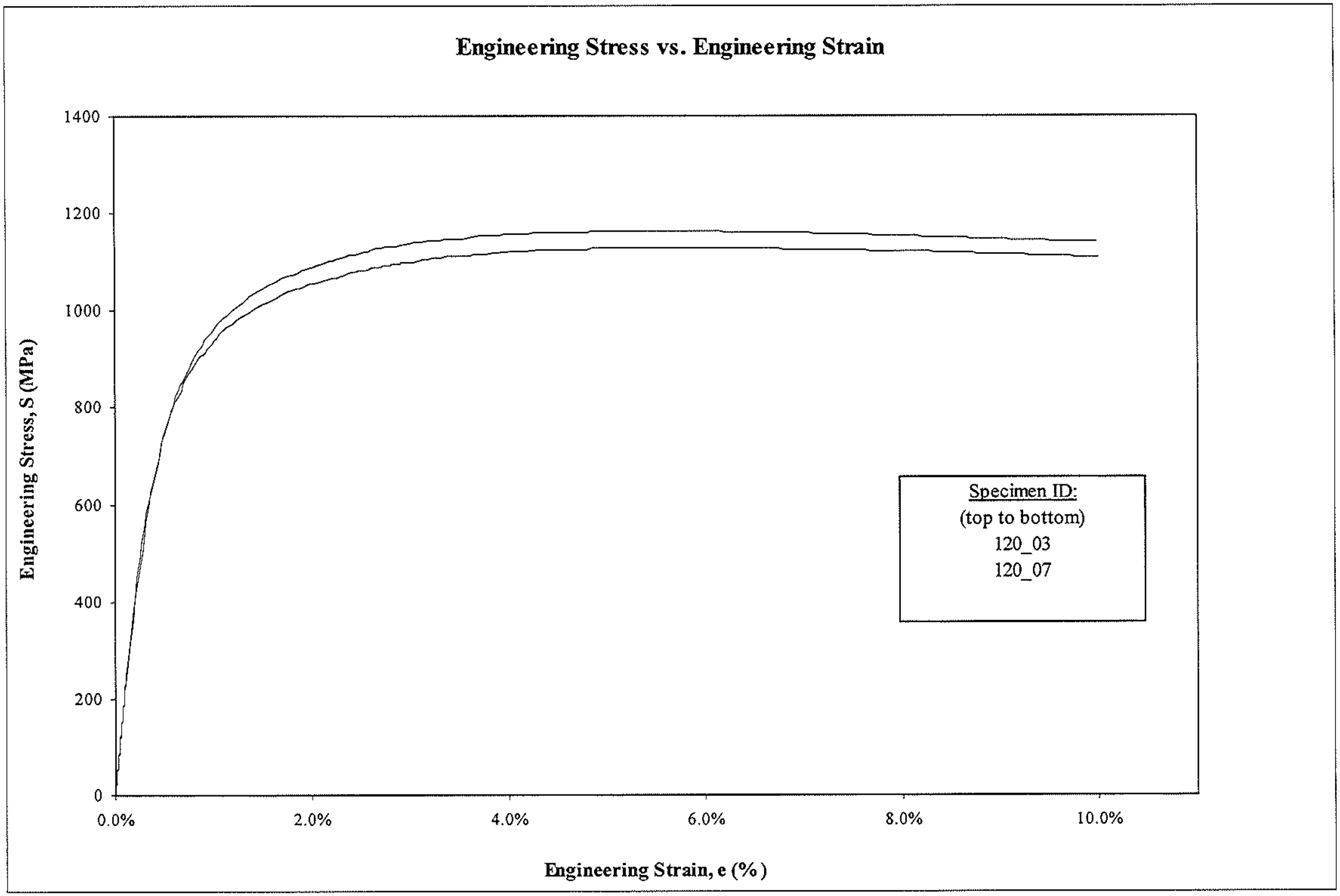

Figure 5: Monotonic stress-strain curves

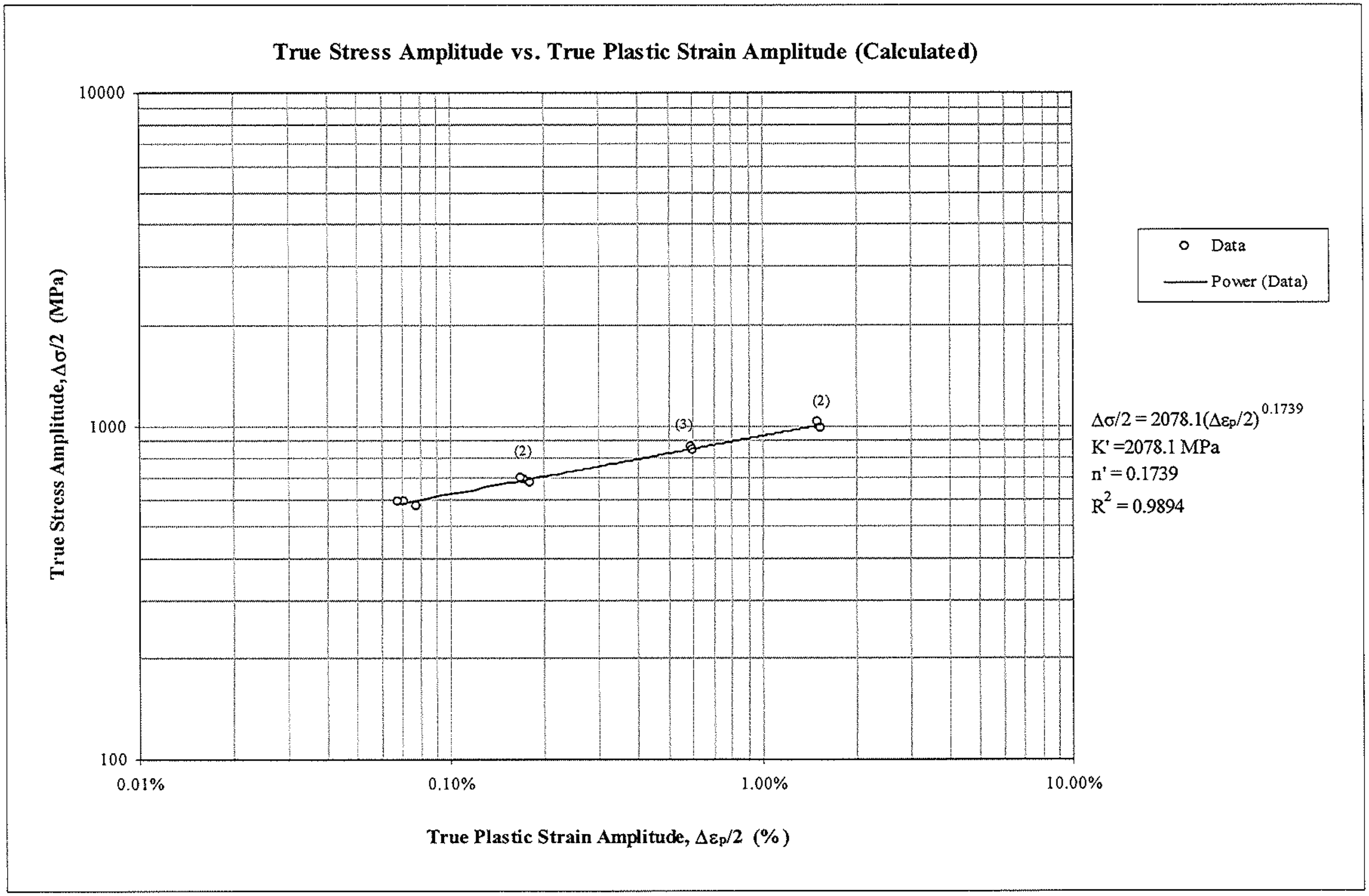

Figure 6: True stress amplitude versus true plastic strain amplitude (calculated)

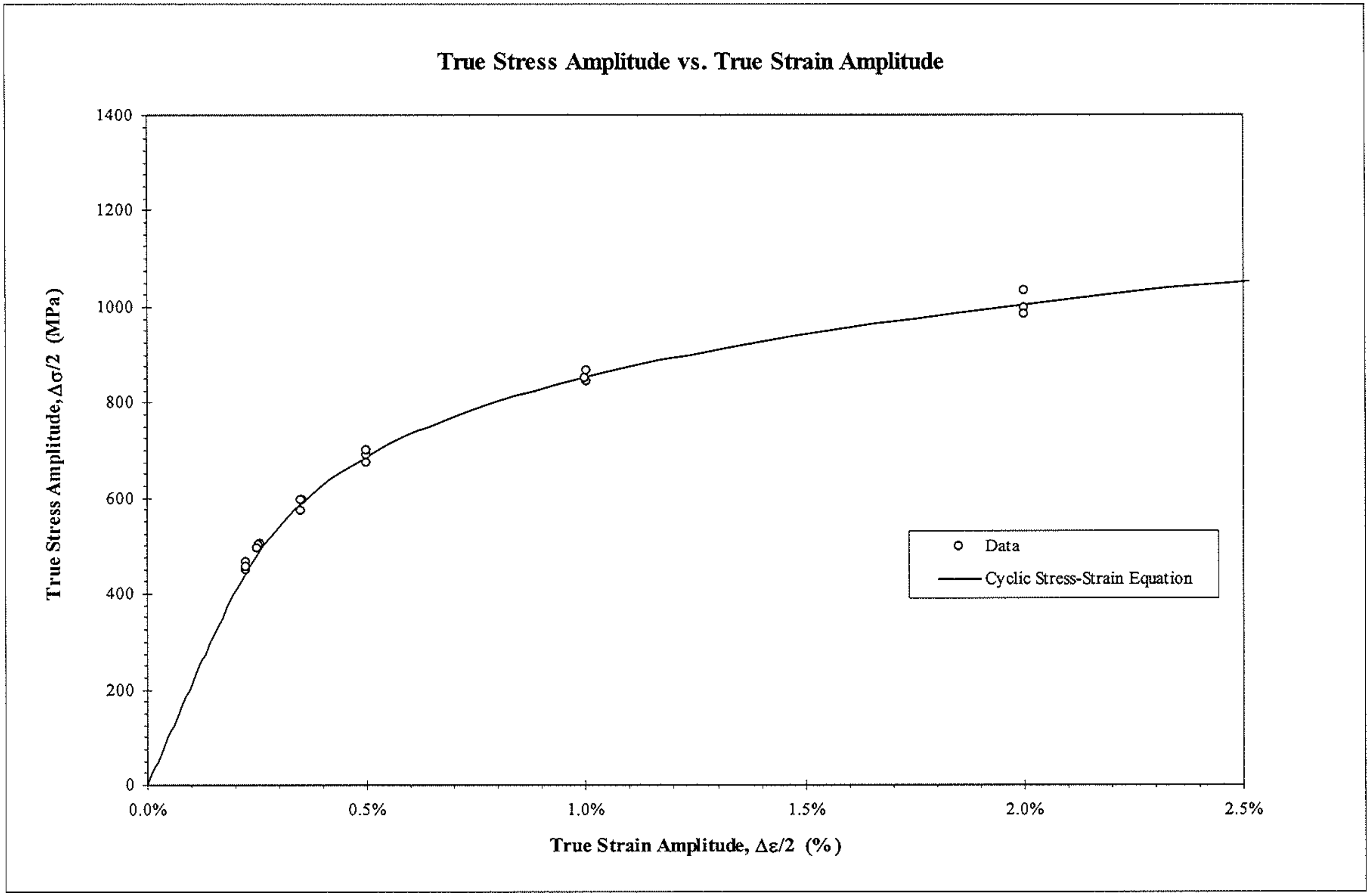

Figure 7: True stress amplitude versus true strain amplitude

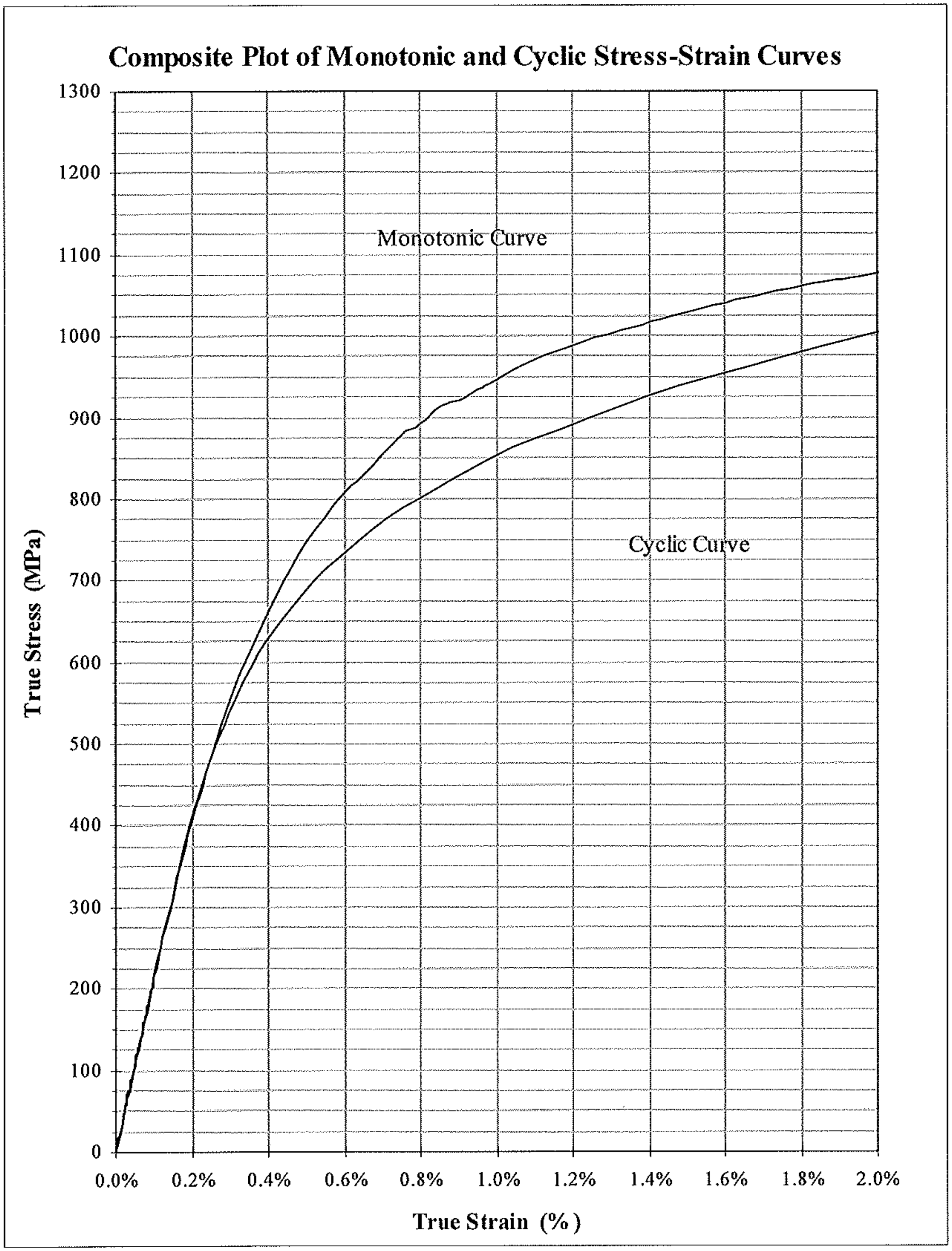

Figure 8: Composite plot of cyclic and monotonic stress-strain curves

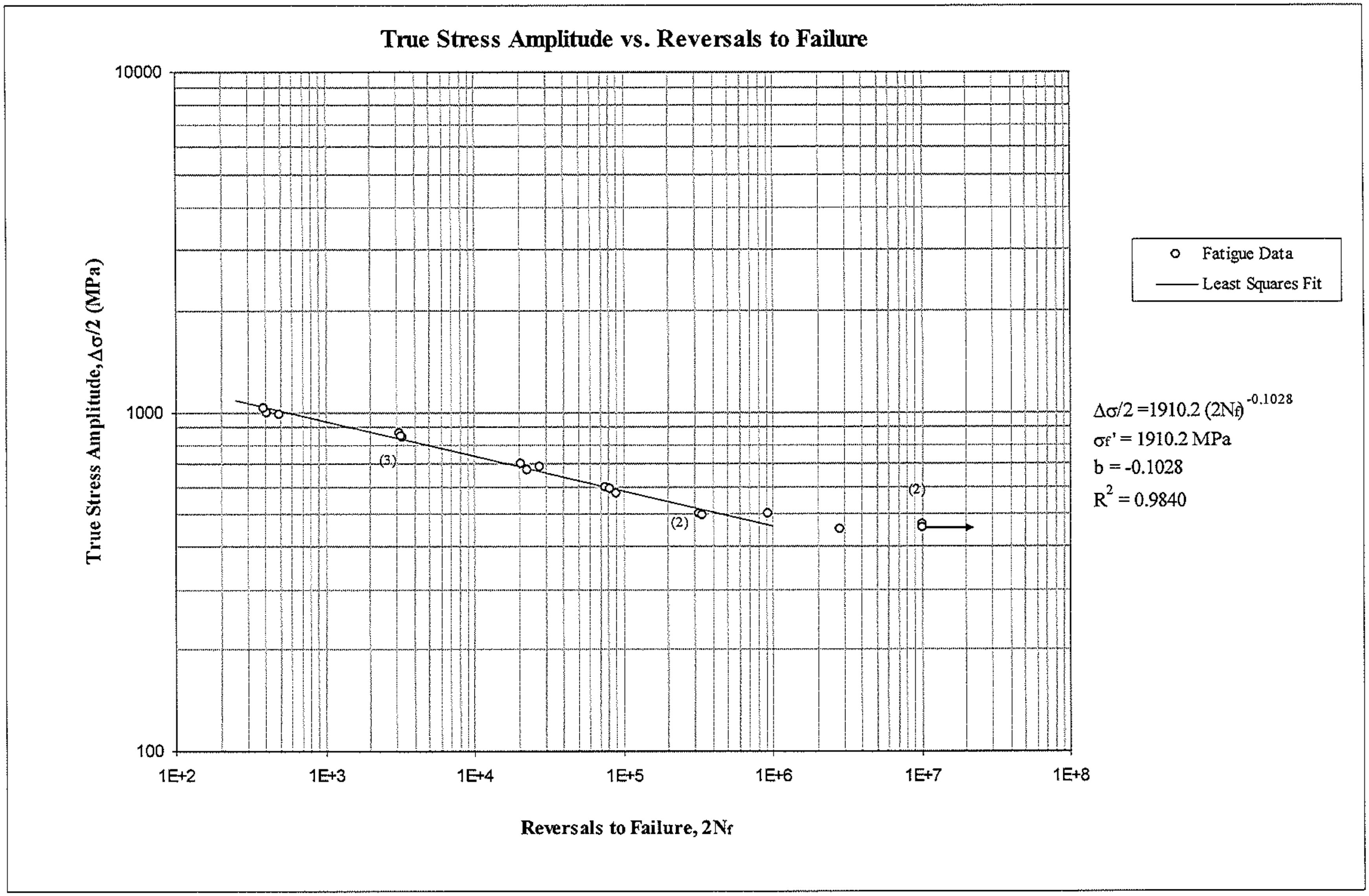

Figure 9: True stress amplitude versus reversals to failure

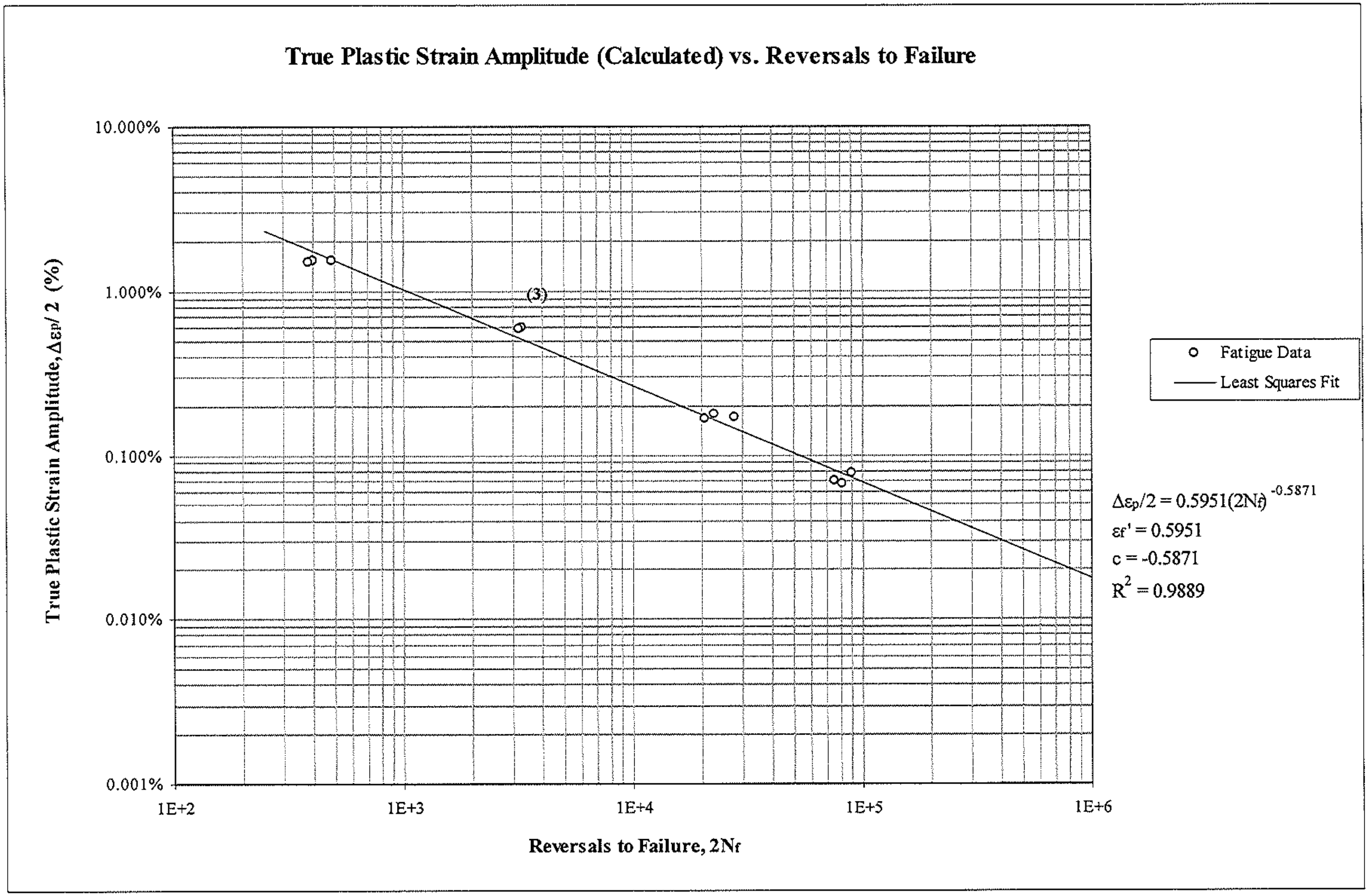

Figure 10: True plastic strain amplitude (calculated) versus reversals to failure

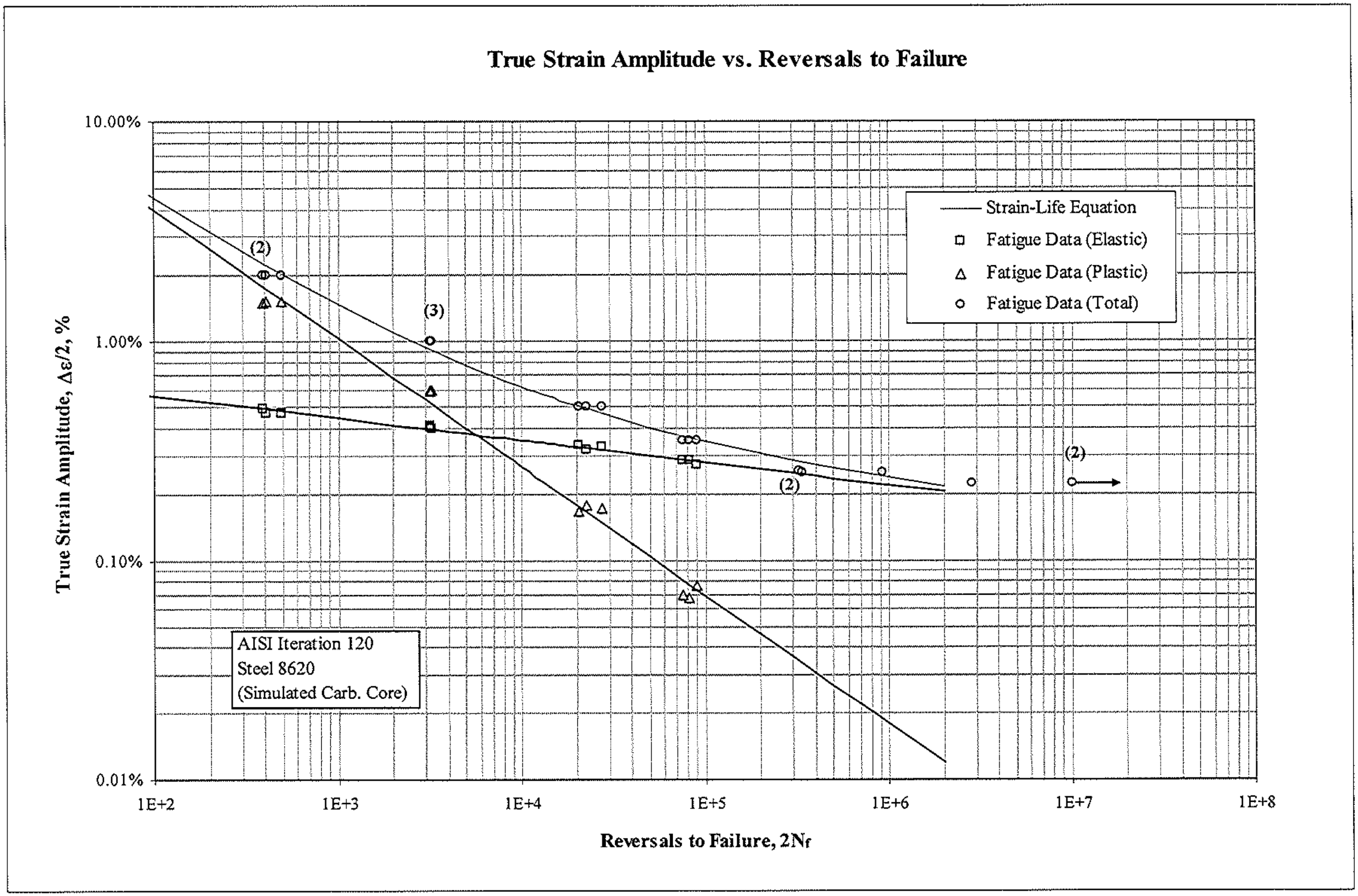

Figure 11: True strain amplitude versus reversals to failure

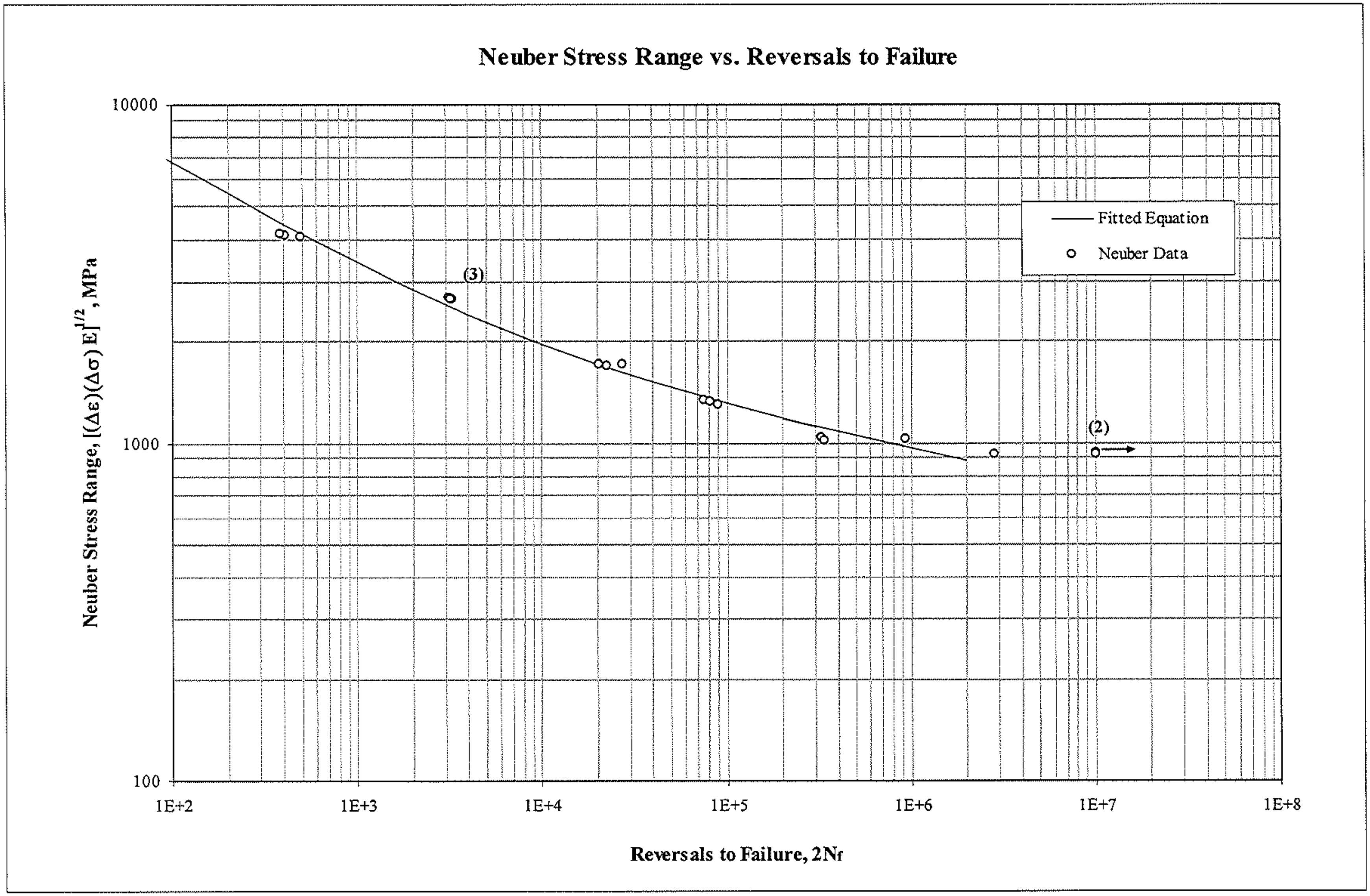

Figure 12: Neuber stress range versus reversals to failure

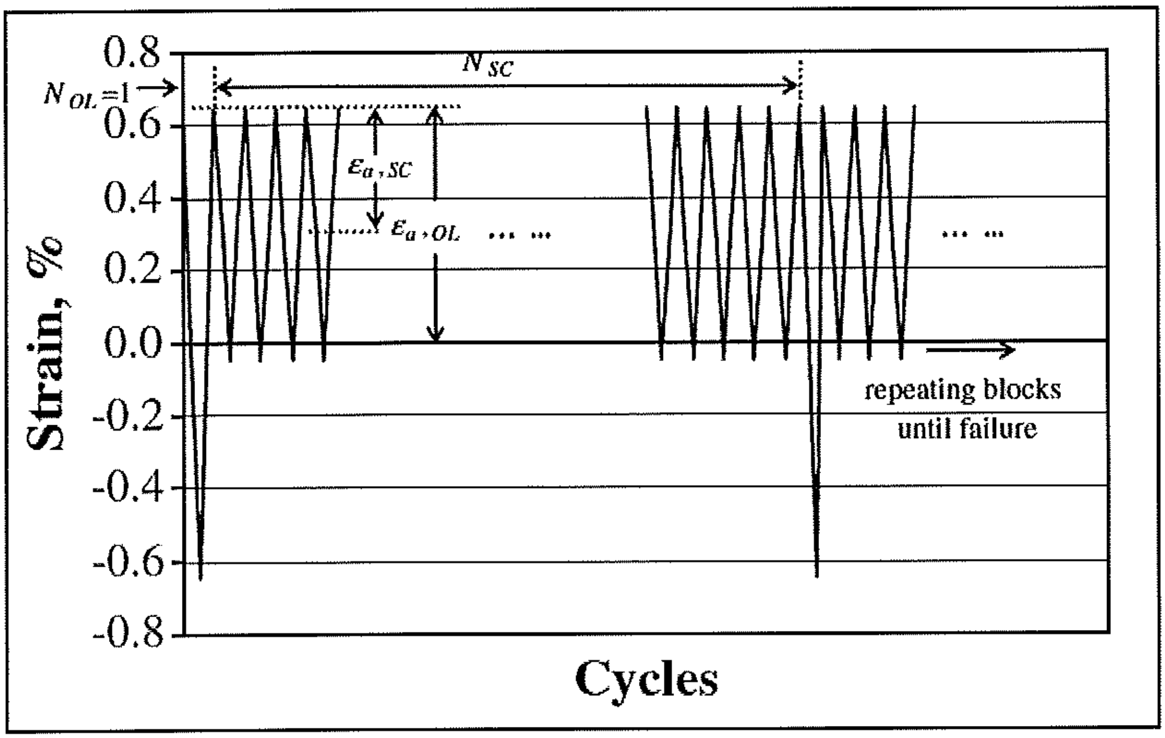

Figure 13: Periodic overload history

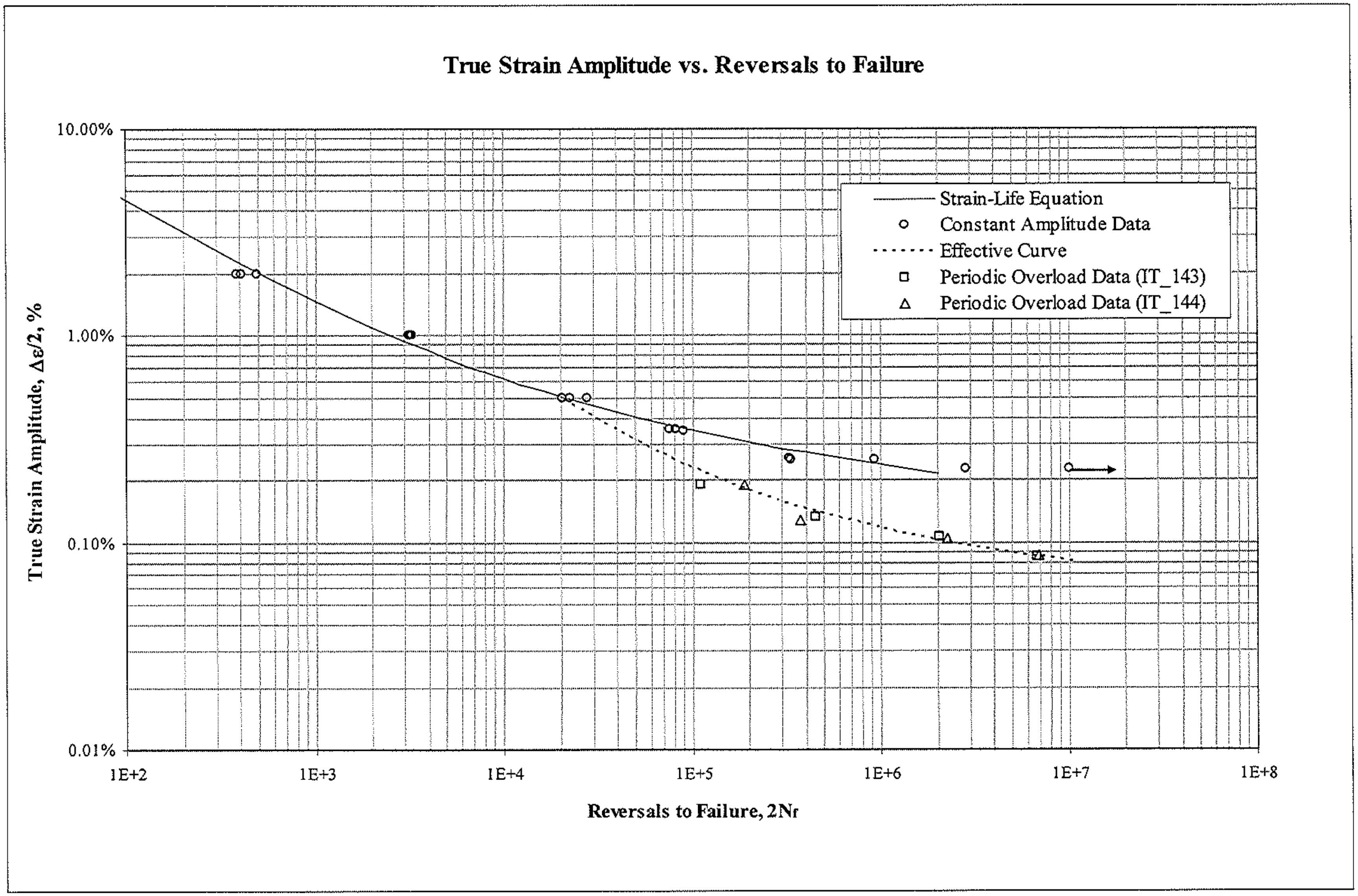

Figure 14: Periodic overload data superimposed with constant amplitude fatigue data

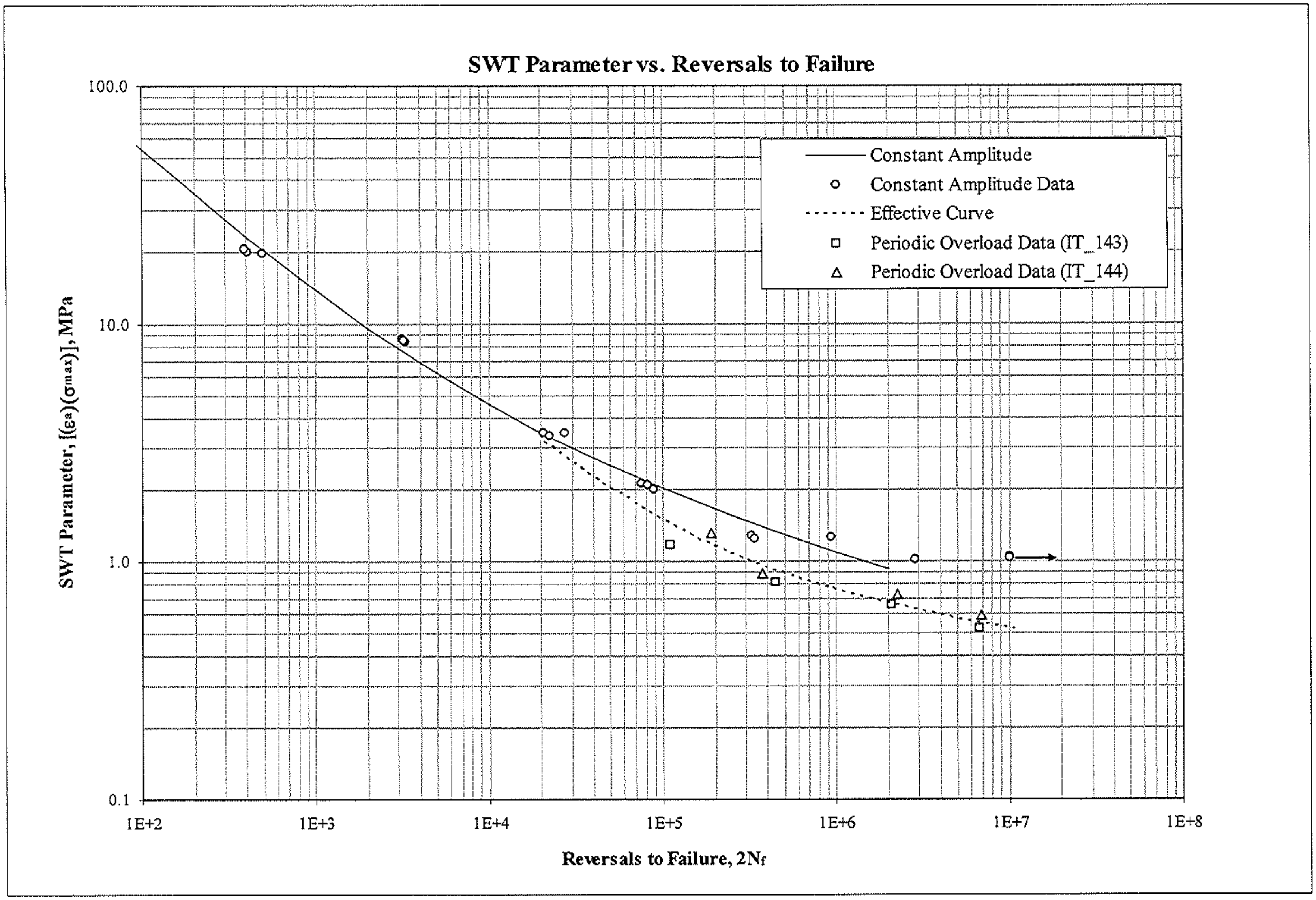

Figure 15: SWT parameter versus reversals to failure. Periodic overload data superimposed on constant amplitude data

REFERENCES

[1] ASTM Standard E606-92, "Standard Practice for Strain-Controlled Fatigue Testing," Annual Book of ASTM Standards, Vol. 03.01, 2004, pp. 593-606.

[2] ASTM Standard E83-02, "Standard Practice for Verification and Classification of Extensometers," Annual Book of ASTM Standards, Vol. 03.01, 2004, pp. 232-244.

[3] ASTM Standard E1012-99, "Standard Practice for Verification of Specimen Alignment Under Tensile Loading," Annual Book of ASTM Standards, Vol. 03.01, 2004, pp. 763-770.

[4] ASTM Standard E8-04, "Standard Test Methods for Tension Testing of Metallic Materials," Annual Book of ASTM Standards, Vol. 03.01, 2004, pp. 62-85.

[5] ASTM Standard E739-91, "Standard Practice for Statistical Analysis of Linear or Linearized Stress-Life (S-N) and Strain-Life (ε-N) Fatigue Data," Annual Book of ASTM Standards, Vol. 03.01, 1995, pp. 670-676.

[6] ASTM Standard E646-00, "Standard Test Method for Tensile Strain-Hardening Exponents (n-values) of Metallic Sheet Materials," Annual Book of ASTM Standards, Vol. 03.01, 2004, pp. 619-626.

[7] Stephens R. I., Fatemi A., Stephens R. R. and Fuchs H. O., "*Metal Fatigue in Engineering*", Second edition, Wiley Interscience, 2000.

APPENDIX A

Table A-1: Summary of monotonic tensile test results

Specimen ID	D_o, mm (in)	D_f, mm (in)	L_o, mm (in)	L_f, mm (in)	R, mm (in)	E, Gpa (ksi)	YS (offset=0.2%), Mpa (ksi)	S_u, Mpa (ksi)	K, Mpa (ksi)	n	%EL	%RA	ε_f, %	σ_f, Mpa (ksi)
120_07	5.029 (0.1980)	3.442 (0.1355)	7.020 (0.2764)	9.38 (0.3693)	2.794 (0.1100)	211.6 (30,685)	795.5 (115.4)	1128.4 (163.7)	2020.5 (293.0)	0.1561	33.6%	53.2%	75.9%	1618.1 (234.7)
120_03	5.131 (0.2020)	3.683 (0.1450)	7.260 (0.2858)	9.97 (0.3925)	3.112 (0.1225)	209.0 (30,310)	796.0 (115.4)	1162.1 (168.5)	2244.2 (325.5)	0.1741	37.3%	48.5%	66.3%	1553.4 (225.3)
Average Values						210.3 (30,497)	795.8 (115.4)	1145.2 (166.1)	2132.3 (309.3)	0.1651	35.5%	50.8%	71.1%	1585.7 (230.0)

Table A-2: Summary of constant amplitude completely reversed fatigue test results

Specimen ID	Test control mode	Test freq., Hz	E, GPa (ksi) [e]	At midlife ($N_{50\%}$) E', GPa (ksi)	$\Delta\varepsilon/2$, %	$\Delta\varepsilon_p/2$ (calculated), %	$\Delta\varepsilon_p/2$ (measured), %	$\Delta\sigma/2$, MPa (ksi)	σ_m, MPa (ksi)	$2N_{50\%}$, [a] reversals	$(2N_f)_{10\%}$, [b] reversals	$(2N_f)_{50\%}$, [c] reversals	Failure location [d]
120_05	strain	0.2	211.2 (30,630)	214.5 (31,106)	2.001%	1.527%	1.453%	995.7 (144.4)	-5.5 -(0.8)	256	386	404	IGL
120_12	strain	0.2	214.5 (31,116)	212.8 (30,858)	2.000%	1.509%	1.441%	1030.6 (149.5)	-5.9 -(0.9)	256	380	386	IGL
120_14	strain	0.2	203.2 (29,464)	205.6 (29,818)	2.000%	1.532%	1.452%	983.5 (142.6)	-5.6 -(0.8)	256	472	490	IGL
120_19	strain	0.3	212.1 (30,768)	211.3 (30,646)	1.001%	0.589%	0.538%	867.0 (125.7)	-9.3 -(1.3)	1,024	3,152	3,168	IGL
120_16	strain	0.3	202.9 (29,425)	210.6 (30,540)	1.001%	0.599%	0.549%	844.5 (122.5)	-6.2 -(0.9)	1,024	3,192	3,264	IGL
120_13	strain	0.3	198.7 (28,816)	202.3 (29,341)	0.999%	0.595%	0.536%	850.2 (123.3)	-5.9 -(0.9)	1,024	3,064	3,198	IGL
120_24	strain	1.0	205.2 (29,762)	213.1 (30,904)	0.501%	0.172%	0.148%	690.2 (100.1)	-10.3 -(1.5)	8,192	25,796	27,584	IGL
120_11	strain	1.0	214.2 (31,062)	212.3 (30,793)	0.500%	0.167%	0.150%	699.4 (101.4)	0.7 (0.1)	8,192	19,882	20,532	IGL
120_15	strain	1.0	214.1 (31,058)	211.0 (30,609)	0.500%	0.179%	0.156%	675.3 (97.9)	-1.1 -(0.2)	8,192	21,786	22,446	IGL
120_01	strain load	1.4 1.4	206.7 (29,982)	-	0.354%	0.070%	-	596.9 (86.6)	2.1 (0.3)	32,768	-	75,378	IGL
120_30	strain	1.4	199.1 (28,877)	211.1 (30,617)	0.351%	0.067%	0.058%	595.8 (86.4)	41.3 (6.0)	32,768	78,238	81,370	IGL
120_22	strain	1.4	200.5 (29,077)	206.7 (29,977)	0.349%	0.077%	0.061%	573.0 (83.1)	25.7 (3.7)	32,768	73,216	89,296	IGL
120_18	strain load	3.0 3.0	-	-	0.255%	0.016%	-	503.4 (73.0)	1.3 (0.2)	131,072	-	325,116	IGL
120_17	strain load	3.0	207.3 (30,065)	-	0.252%	0.013%	-	502.0 (72.8)	1.3 (0.2)	524,288	-	928,224	IGL
120_06	strain load	3.0	206.5 (29,949)	-	0.251%	0.016%	-	494.1 (71.7)	1.2 (0.2)	131,072	-	335,166	IGL
120_26	load	35.0	-	-	0.225%	0.011%	-	450.3 (65.3)	1.0 (0.1)	1,048,576	-	2,843,664	IGL
120_09	strain load	3.0 35.0	208.8 (30,282)	-	0.225%	0.004%	-	464.0 (67.3)	1.0 (0.2)	-	-	>10,000,000	No Failure
120_20	load	35.0	-	-	0.225%	0.009%	-	454.8 (66.0)	1.0 (0.1)	-	-	>10,000,000	No Failure

[a] $2N_{50\%}$ is defined as the midlife reversal ;

[b] $2(N_f)_{10\%}$ is defined as reversal of 10% load drop

[c] $2(N_f)_{50\%}$ is defined as reversal of 50% load drop or failure

[d] IGL = Inside gage length;

[e] E value was calculated from the first cycle

Table A-3: Summary of the periodic overload fatigue test results

Spec. ID	Test Control Mode [d]	Test Freq. OL/SC (Hz)	E (GPa) [b]	Load history Description											Exp. Life (Blks)	$N_{f, sc(eq)}$ (Cycles)	OL Damage Ratio	Failure Location [a]
				$\varepsilon_{a, SC}$ (%)	$\varepsilon_{m, SC}$ (%)	$\Delta\varepsilon_p/2_{, SC}$ (calculated) (%)	$\sigma_{a, SC}$ (MPa) [c]	$\sigma_{m, SC}$ (MPa) [c]	N_{SC} (Cycles)	$\varepsilon_{a, OL}$ (%)	$\Delta\varepsilon_p/2_{, OL}$ (calculated) (%)	$\sigma_{a, OL}$ (MPa) [c]	$\sigma_{m, OL}$ (MPa) [c]	$N_{f, OL}$ (Cycles)				
119_07	load	1 / 5	-	0.192%	0.420%	0.028%	347.3	264.8	64	0.612%	0.320%	618.4	2.3	8,012	680	55,066	0.210	IGL
120_21	load	1 / 5	193.0	0.192%	0.331%	0.022%	357.5	331.4	64	0.523%	0.191%	697.0	2.3	9,117	1,133	94,659	0.234	IGL
119_13	load	1 / 5	196.7	0.134%	0.438%	0.012%	258.9	354.5	256	0.572%	0.281%	616.1	0.7	8,309	701	225,648	0.205	IGL
120_08	load	1 / 5	209.8	0.129%	0.347%	0.005%	259.7	430.4	256	0.476%	0.146%	695.2	2.3	9,349	607	187,648	0.172	IGL
119_06	load	1 / 5	194.2	0.107%	0.408%	0.008%	208.3	404.2	1,024	0.514%	0.224%	615.0	0.0	8,463	793	1,030,335	0.212	IGL
120_29	load	1 / 5	191.2	0.105%	0.395%	0.006%	208.1	481.8	1,024	0.500%	0.170%	692.5	0.4	9,714	883	1,121,612	0.194	IGL
119_11	load	1 / 35	191.9	0.085%	0.416%	0.006%	167.0	442.7	2,048	0.501%	0.213%	609.7	0.0	9,218	1,246	3,373,822	0.244	IGL
120_25	load	1 / 35	201.9	0.086%	0.436%	0.007%	166.6	520.6	2,048	0.522%	0.195%	687.2	0.0	10,473	1,307	3,432,992	0.220	IGL

[a] IGL = Inside gage length
[b] E value was calculated from the first cycle
[c] All stress values reported are from mid-life
[d] Load-controlled tests were pre-cycled at the OL stress amplitude for 1000 cycles. Damage from the pre-strained cycles is included in the OL damage ratio

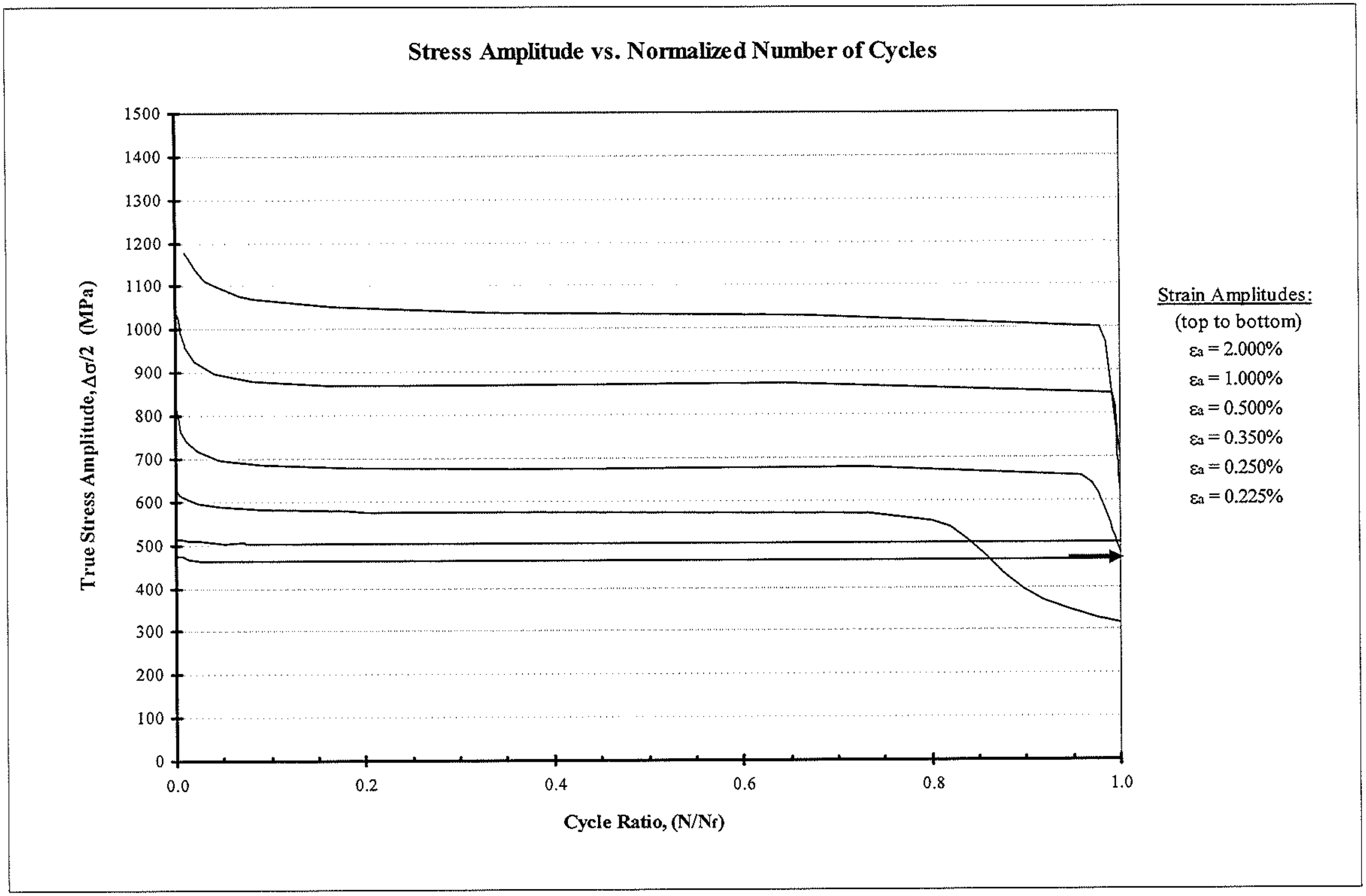

Figure A-1a: True stress amplitude versus normalized number of cycles

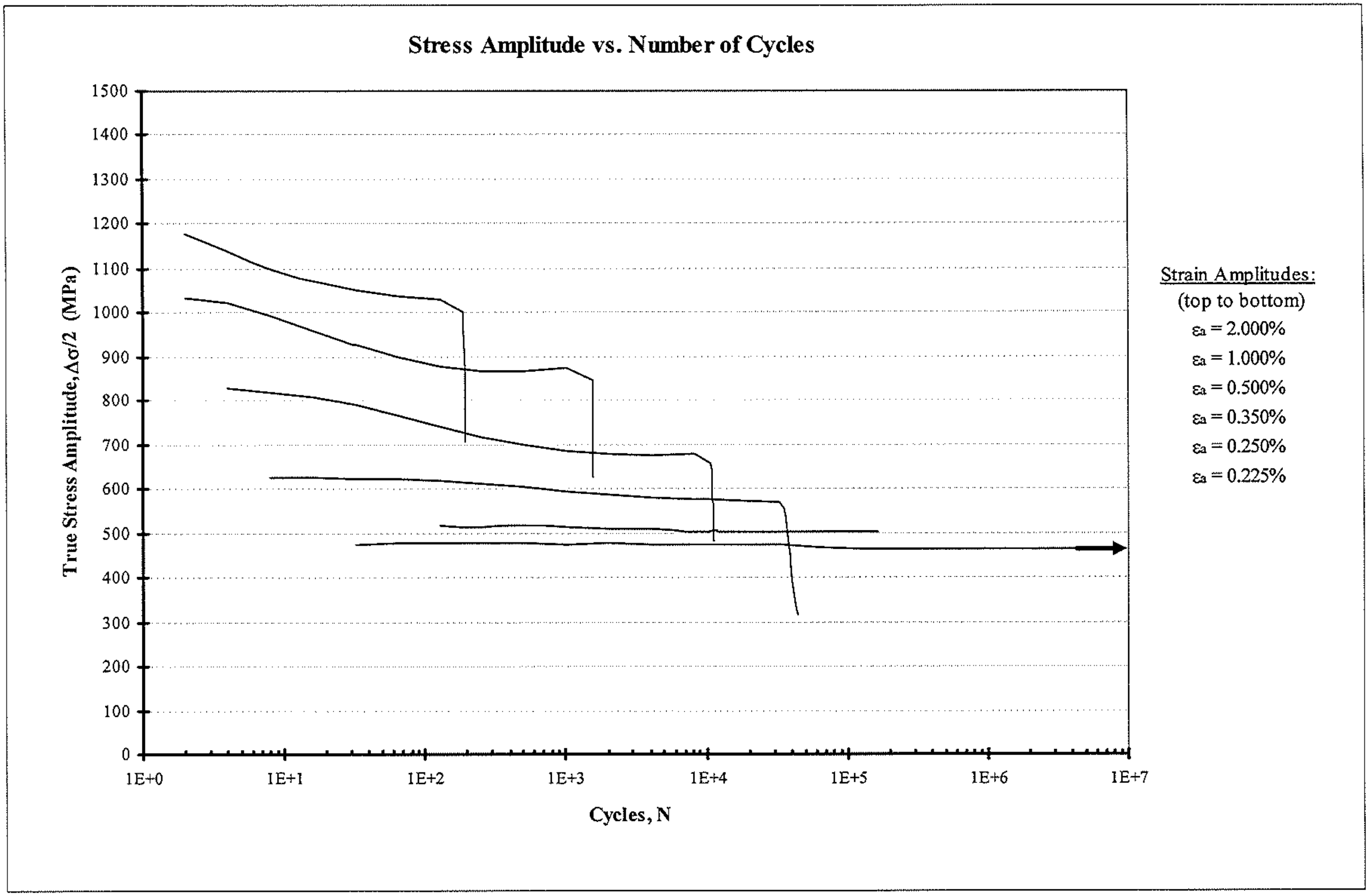

Figure A-1b: True stress amplitude versus number of cycles

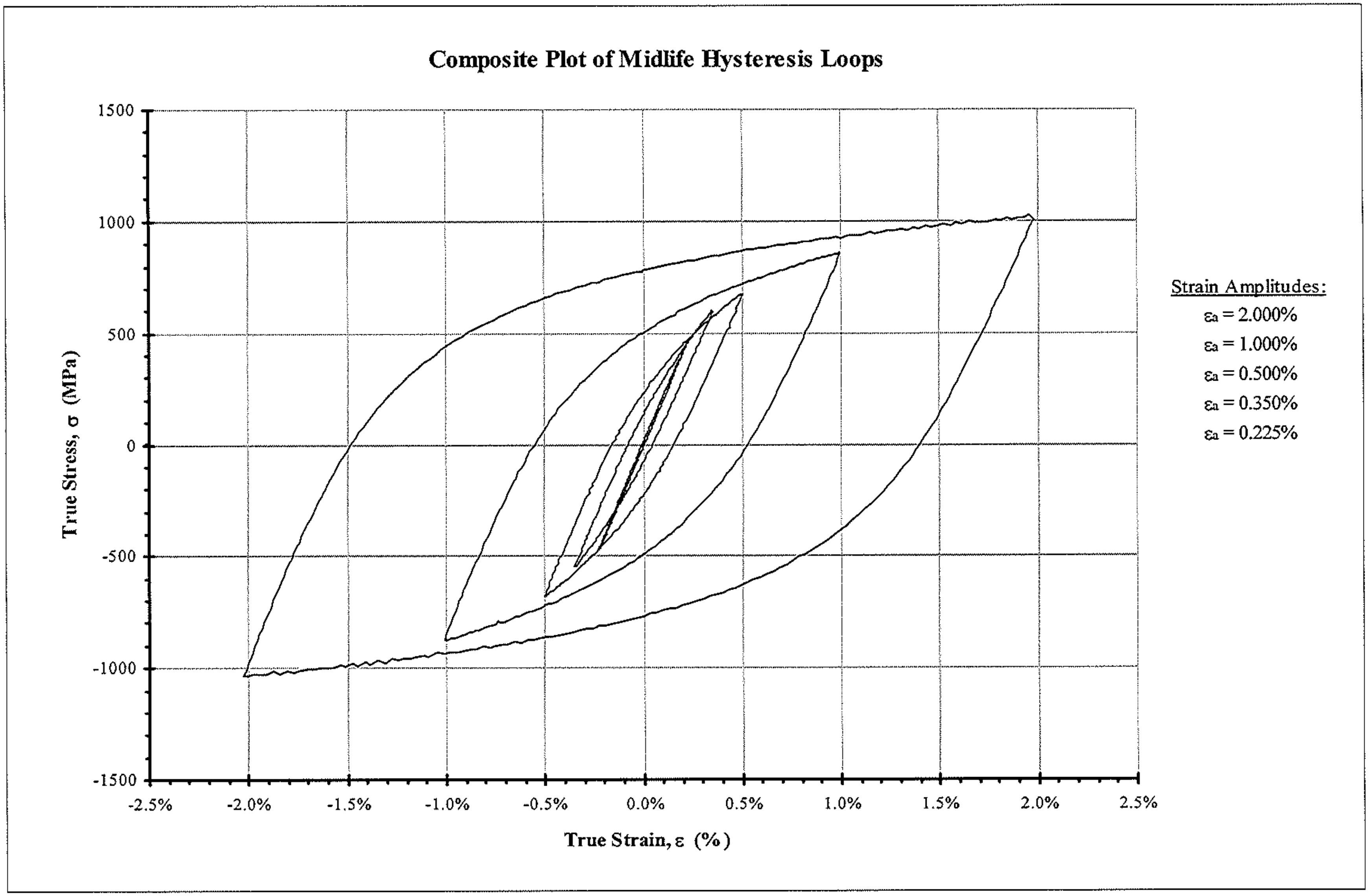

Figure A-2: Composite plot of midlife hysteresis loops

APPENDIX B

CHRYSLER

UAW - Chrysler SPG
SCIENTIFIC LABS & PROVING GROUNDS

Materials Engineering Summary Report

LTR Number: 135765

From:	**Peter Bauerle**	**Phone:**	**776-7387**
Location:	**CTC**		

Lab(s):	**Metallography** **Mechanical Properties**	**Completed:**	**4/28/2010**

Subject/Part Name: Tensile Specimen - Iteration 120-26
Approver: Theresa Klix
Originator: Peter Bauerle
Originator Phone: 248-576-7387
Number of Parts: 1
Nature of Work: Pilot, Mule, Program Development Issue
Vendor:
Plant:
P/N:
MS:
PS:

History of Part

The sample represents a tensile specimen from AISI iteration 120 that has been submitted for metallographic evaluation. The analysis will simply use a longitudinal section prepared from the grip end for use in the evaluation of the microstructure and hardness traverse.

Purpose

The purpose of this LTR is to perform a metallographic analysis and a hardness check on the grip section of the tensile specimen.

Metallography - 135765

General Microstructure Description (Performed By: Xichen Sun)

Sample surface profile

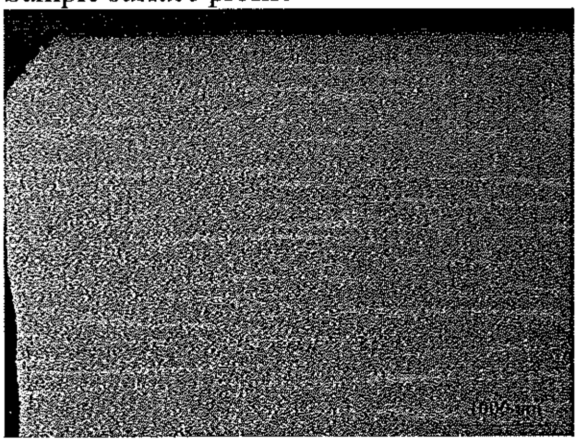

Core and surface showing same microstructure – martensite + transformed products

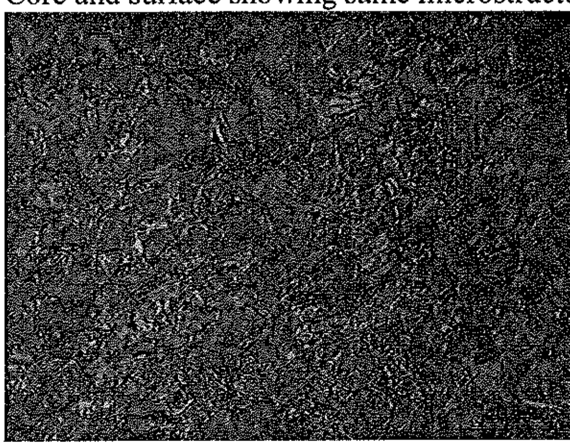

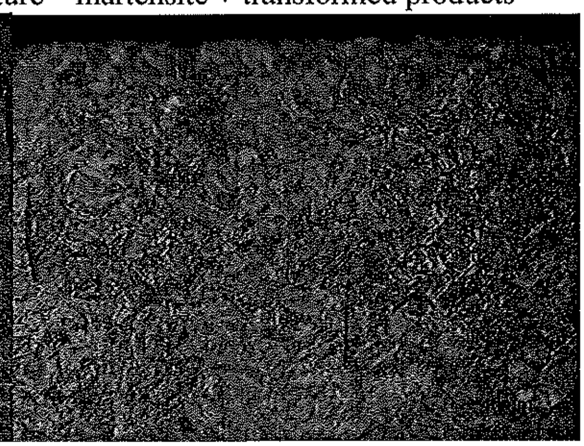

Core X500 Surface X500

Mechanical Properties - 135765

Hardness - Rockwell (Performed By: Greg Cornelissen)

Grip section (surface hardness) - 37.9 HRC 39.3 HRC 37.4 HRC

Hardness - Micro (Performed By: Greg Cornelissen)

Newage Microhardness Tester – 1000gf

Microhardness traverse starting from the edge of the part and staggered in increments of .005" to a depth of .030" followed by increments .010" to the core. Aim hardness range is 35 – 40 HRC.

.005"	37.3 HRC
.010"	35.3 HRC
.015"	39.2 HRC
.020"	36.0 HRC
.025"	35.3 HRC
.030"	35.6 HRC
.040"	37.6 HRC
.050"	39.2 HRC
.060"	35.1 HRC
.070"	37.1 HRC
.080"	34.9 HRC
.090"	35.9 HRC
.100"	37.4 HRC